AIP Journal of Applied Physics

Energy band alignment of atomic layer deposited HfO2 oxide film on epitaxial (100)Ge, (110)Ge, and (111)Ge layers

Mantu K. Hudait and Yan Zhu

Citation: Journal of Applied Physics **113**, 114303 (2013); doi: 10.1063/1.4795284
View online: http://dx.doi.org/10.1063/1.4795284
View Table of Contents: http://scitation.aip.org/content/aip/journal/jap/113/11?ver=pdfcov
Published by the AIP Publishing

Energy band alignment of atomic layer deposited HfO_2 oxide film on epitaxial (100)Ge, (110)Ge, and (111)Ge layers

Mantu K. Hudait[a] and Yan Zhu
Advanced Devices & Sustainable Energy Laboratory (ADSEL), Bradley Department of Electrical and Computer Engineering, Virginia Tech, Blacksburg, Virginia 24061, USA

(Received 26 December 2012; accepted 28 February 2013; published online 18 March 2013)

Crystallographically oriented epitaxial Ge layers were grown on (100), (110), and (111)A GaAs substrates by *in situ* growth process using two separate molecular beam epitaxy chambers. The band alignment properties of atomic layer hafnium oxide (HfO_2) film deposited on crystallographically oriented epitaxial Ge were investigated using x-ray photoelectron spectroscopy (XPS). Valence band offset, ΔE_v values of HfO_2 relative to (100)Ge, (110)Ge, and (111)Ge orientations were 2.8 eV, 2.28 eV, and 2.5 eV, respectively. Using XPS data, variation in valence band offset, $\Delta E_V(100)Ge > \Delta E_V(111)Ge > \Delta E_V(110)Ge$, was obtained related to Ge orientation. Also, the conduction band offset, ΔE_c relation, $\Delta E_c(110)Ge > \Delta E_c(111)Ge > \Delta E_c(100)Ge$ related to Ge orientations was obtained using the measured bandgap of HfO_2 on each orientation and with the Ge bandgap of 0.67 eV. These band offset parameters for carrier confinement would offer an important guidance to design Ge-based p- and n-channel metal-oxide field-effect transistor for low-power application. © *2013 American Institute of Physics*. [http://dx.doi.org/10.1063/1.4795284]

I. INTRODUCTION

A combination of high-κ gate dielectric with high mobility III-V and Ge channel materials has been explored for transistor miniaturization and to enhance transistor performance at low supply voltage operation.[1] One attractive approach is to replace the Si channel with high intrinsic hole mobility Ge for p-channel and low effective carrier mass III-V material for n-channel material.[2–5] Alternative approach is different surface orientations to improve carrier mobility[6–9] and optimal channel direction for device speed.[10–14] Recently, semiconductor industry was replaced SiO_2 gate oxide by hafnium-based gate dielectric on Si complementary metal oxide semiconductor (CMOS) technology and demonstrated superior microprocessor performance compared to SiO_2 gate oxide.[15] A combination of HfO_2 high-κ gate dielectric with high mobility Ge would provide an opportunity for interface engineering and tailoring transistor properties. Moreover, HfO_2 high-κ dielectric should have a valence and conduction band discontinuity larger than 1 eV relative to the Ge channel material[16] to reduce leakage currents due to tunneling through the barrier at the interface between the HfO_2 and the Ge layer.

Significant research on the high-κ gate dielectrics HfO_2,[17,18] ZrO_2,[19] Al_2O_3,[20–22] Y_2O_3,[23] and germanium-oxynitride[24] has been studied on the (100)Ge metal-oxide semiconductor (MOS) devices. Although excellent device performances were achieved using high-κ gate dielectrics on bulk (100)Ge and oxide/(100)Ge band alignment properties, little attention has been devoted on the integration of high-κ gate dielectrics on the epitaxial (110)Ge, (111)Ge, and the associated energy band alignment at each interface. Moreover, finding a *common high-κ gate dielectric* on epitaxial (100)Ge, (110)Ge, and (111)Ge layer is essential to eliminate the formation of high density intrinsic defects with energy levels in the semiconductor band gap[25] due to poor quality native oxides, resulting in Fermi level pinning[26] at the oxide-semiconductor interface. *In this paper*, we have investigated and compared the band alignment properties between the atomic layer deposited HfO_2 oxide film on the crystallographically oriented epitaxial Ge layer grown on (100)GaAs, (110)GaAs, and (111)A GaAs substrates using x-ray photoelectron spectroscopy (XPS) measurement. Furthermore, the use of Ge orientations for device applications as well as Ge surface orientation on interface properties is essential for designing p-channel and n-channel Ge metal-oxide semiconductor field-effect transistors (MOSFETs). In this study, we have demonstrated both valance band and conduction band offsets larger than 2 eV on crystallographically oriented Ge layer.

II. EXPERIMENTAL

Undoped epitaxial Ge layers were grown by *in situ* growth process on (100), (110), and (111)A epi-ready GaAs substrates using separate solid source molecular beam epitaxy (MBE) growth chambers for Ge and III-V materials, connected via ultra-high vacuum transfer chamber. Substrate oxide desorption was done at ~680 °C for (100)/6°-oriented GaAs, ~580 °C for (110)-oriented GaAs, and ~550 °C for (111)A-oriented GaAs substrates under an arsenic overpressure of $\sim 1 \times 10^{-5}$ torr in a III-V MBE chamber. Reflection high energy electron diffraction patterns were recorded for each step of the growth process. A 0.2 μm thick undoped GaAs layer was grown on each GaAs substrate prior to the deposition of Ge epilayer grown at 400 °C on each orientation. The details of the growth procedure and structural properties can be found elsewhere.[27,28] The 1 nm and 5 nm HfO_2 films were grown by atomic layer deposition (ALD) in a Cambridge NanoTech system on epitaxial (100)Ge, (110)Ge, and (111)Ge using a tetrakis(dimethylamino)hafnium compound

[a]Author to whom correspondence should be addressed. Electronic mail: mantu.hudait@vt.edu. Tel.: (540) 231-6663. Fax: (540) 231-3362.

as Hf precursor and H_2O as oxygen source. All Ge epilayers were wet etched to ~5 nm using $NH_4OH:H_2O_2:H_2O$ (2:1:200 volume ratio) prior loading to ALD chamber for HfO_2 deposition. During the HfO_2 growth, the surface temperature of all Ge samples and Hf precursor temperature were kept constant at 250 °C and 75 °C, respectively. All three Ge layers were placed in each run for HfO_2 deposition thickness of 1 nm or 5 nm.

The band alignment properties of HfO_2/(100)Ge, HfO_2/(110)Ge, and HfO_2/(111)Ge structures were investigated using a PHI Quantera SXM XPS system with a monochromated Al-$K\alpha$ (energy of 1486.7 eV) x-ray source. The Ge 3d and Hf 4f core level (CL) binding energy spectra as well as Ge and Hf valence band (VB) binding energy spectra for all orientations were collected with a pass energy of 26 eV and an exit angle of 45°. The CL energy position was defined as the center of the peak width at the half of the peak height (i.e., full width at half maximum). The bandgap of the HfO_2 film, the CL, and valence electrons emitted from each orientation determined from XPS measurement will allow to determine the valence band offset of HfO_2 relative to (100)Ge, (110)Ge, and (111)Ge films by the method described in Ref. 29. The angle integrated photoelectron energy distribution curves for the valence band maximum (VBM), the Ge 3d, and Hf 4f core levels spectra were recorded. The binding energy was corrected by adjusting the carbon 1s core-level peak position to 285.0 eV for each sample surface. This work provided the detailed study on the band alignment properties of the HfO_2 relative to the epitaxial (100)Ge, (110)Ge, and (111)Ge layers along with the offset values of Ge on off-oriented GaAs substrates, recently demonstrated in Ref. 28.

III. RESULTS AND DISCUSSION

The valence band offset, ΔE_v of 2.8 ± 0.1 eV between the HfO_2 and the (100)Ge was studied by several researchers using different deposition methods of HfO_2.[17] Conduction band offset, ΔE_c varying from 2.0 to 2.2 eV was found[17] and the reason was partly due to the measurement errors associated with the bandgap of HfO_2 layer. These band discontinuities play a central role on the electrical transport properties of MOSFET devices, since sufficient band offset barriers were needed to suppress the tunneling leakage current for both electrons and holes. However, the experimental band offset values on the (110)Ge and (111)Ge epitaxial layers would provide better understanding into the electrical transport properties of the p-channel and n-channel MOSFET, respectively, since the reported hole mobility is higher on (110)Ge and electron mobility on (111)Ge.

A. HfO_2/(100)Ge heterointerface

In order to determine the ΔE_v and ΔE_c at the HfO_2/(100)Ge heterointerface, XPS spectra were collected from the following 3 samples: (1) (100)Ge epitaxial layer, (2) 5 nm thick HfO_2 film on (100)Ge, and (3) interface of 1 nm HfO_2 on (100)Ge layer. Figures 1(a) and 1(b) show the Ge 3d CL (E^{Ge}_{Ge3d}) spectrum and VBM (E^{Ge}_{VBM}) of (100)Ge film as well as Hf 4f CL (E^{Hf}_{Hf4f}) spectrum and VBM (E^{Hf}_{VBM}) of 5 nm

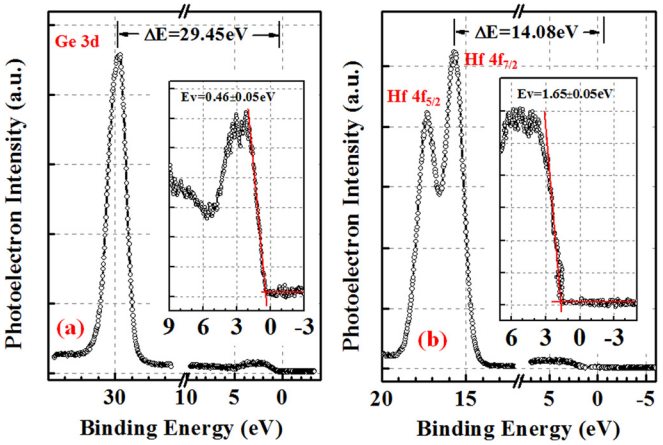

FIG. 1. XPS spectra of (a) Ge 3d core level (E^{Ge}_{Ge3d}) and valence band maximum, VBM (E^{Ge}_{VBM}) of (100)Ge film; (b) Hf 4f core level (E^{Hf}_{Hf4f}) spectrum and VBM (E^{Hf}_{VBM}) of 5 nm HfO_2 film.

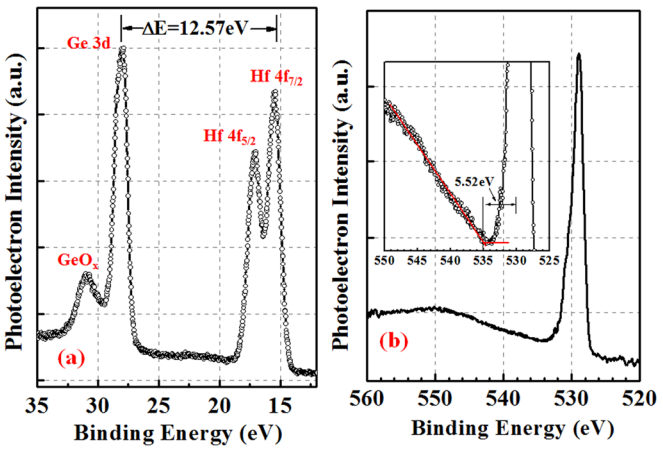

FIG. 2. XPS spectra of (a) Ge 3d (E^{Ge}_{Ge3d}) and Hf 4f core level (E^{Hf}_{Hf4f}) spectra of 1 nm thin HfO_2 film/(100)Ge interface, and (b) shows the core level spectrum of 5 nm HfO_2 film. The band gap of HfO_2 was determined to be 5.52 ± 0.1 eV.

HfO_2 film, respectively. Figure 2(a) shows the Ge 3d CL (E^{Ge}_{Ge3d}) and Hf 4f CL (E^{Hf}_{Hf4f}) spectrum of 1 nm HfO_2 on (100)Ge interface. The ΔE_v at the HfO_2/(100)Ge heterointerface was determined using these measured CL spectra with the following equation:[29]

$$\Delta E_V = \left(E^{Ge}_{Ge3d} - E^{Ge}_{VBM}\right)^{Ge} - \left(E^{Hf}_{Hf4f} - E^{Hf}_{VBM}\right)^{5\mathrm{nm}HfO_2} - \left(E^{Ge}_{Ge3d} - E^{Hf}_{Hf4f}\right)^{1\mathrm{nm}HfO_2/Ge\,\mathrm{interface}}. \quad (1)$$

Finally, the ΔE_c at the HfO_2/(100)Ge interface was determined from the following equation:

$$\Delta E_C = E^{HfO_2}_g - E^{Ge}_g - \Delta E_V, \quad (2)$$

where $E^{HfO_2}_g$ and E^{Ge}_g are the bandgaps of HfO_2 determined from Fig. 2(b) and Ge, respectively.

The position of the Ge 3d peak centroid from the XPS measurement was found to be 30.05 ± 0.05 eV as shown in Fig. 1(a). This value was obtained by measuring the center

of the peak width at half of the peak height after Shirley background subtraction. The error bar we defined in this paper is due to the scatter of VB spectra during the fitting of VBM position and considering the linearity and stability of the energy scale of the XPS binding energy spectrum. The VBM values are determined by linear extrapolation of the leading edge to the base line of the VB spectra recorded on the bulk HfO_2 and thick Ge film to the base lines. Truly, the VBM value is sensitive to the choice of points on the leading edge used to obtain the regression line.[30,31] Several different sets of points were selected over the linear region of the leading edge to perform regressions, and the uncertainty of ΔE_v and ΔE_c values were found to be in the range of 0.05-0.1 eV in the present work. Figure 1(a) shows the VBM for the (100)Ge film. The energy difference between the Ge 3d centroid and the (100)Ge VBM was measured to be 29.45 ± 0.05 eV. Similarly, the energy difference between the Hf 4f centroid and the Hf VBM was found to be 14.08 ± 0.05 eV for 5 nm HfO_2 film. For 1 nm HfO_2 film on (100)Ge, the energy difference between the Ge 3d centroid and the Hf 4f core lines was determined to be 12.57 ± 0.05 eV. Using these measured data and Eq. (1), the measured value of ΔE_v for the HfO_2/(100)Ge interface was determined to be 2.8 ± 0.05 eV. Here, we have selected Hf $4f_{7/2}$ CL spectra than Hf $4f_{5/2}$ since the binding energy separation between the Hf $4f_{7/2}$ and the Hf $4f_{5/2}$ peaks is fixed to be 1.7 eV. As a result, the band offset value would not change if we select Hf $4f_{5/2}$ as the CL binding energy peak.

In order to determine the ΔE_C for the HfO_2 relative to (100)Ge heterointerface, the precise determination of the bandgap of HfO_2 is essential. Figure 2(b) shows the CL spectrum from 5 nm thick HfO_2 film and the band gap was determined to be 5.52 ± 0.1 eV. The ΔE_C can be calculated based on the measured ΔE_v and the difference in bandgaps of HfO_2 and Ge, where $\Delta E_g = \Delta E_v + \Delta E_c$. Using Eq. (2), the ΔE_c was calculated to be 2.05 ± 0.1 eV using the bandgap of Ge 0.67 eV, the measured value of ΔE_v, and the measured bandgap of HfO_2. These offset values are similar to those obtained by several researchers on ALD HfO_2/(100)Ge interface.[17,32] These results also suggest that the barrier height of HfO_2/(100)Ge was large enough to obtain low leakage current using HfO_2 as high-κ gate dielectric on (100)Ge. Table I shows the CL to VBM binding-energy difference and the resulting band offsets on (100)Ge epitaxial layer.

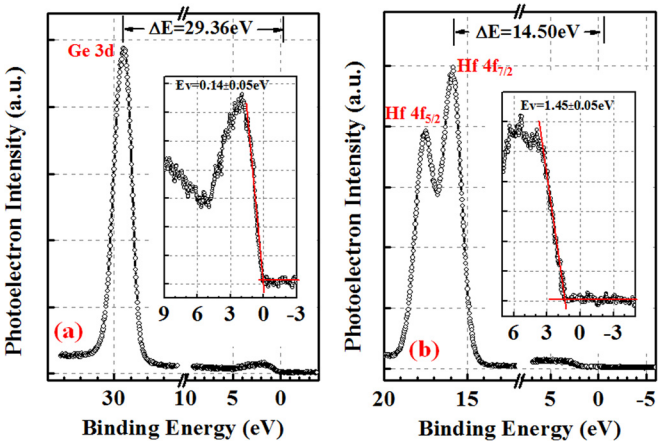

FIG. 3. XPS spectra of (a) Ge 3d core level (E^{Ge}_{Ge3d}) and valence band maximum, VBM (E^{Ge}_{VBM}) of (110)Ge film; (b) Hf 4f core level (E^{Hf}_{Hf4f}) spectrum and VBM (E^{Hf}_{VBM}) of 5 nm HfO_2 film.

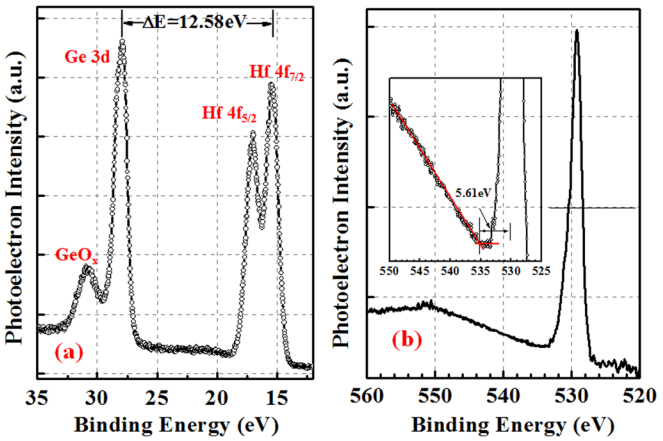

FIG. 4. XPS spectra of (a) Ge 3d (E^{Ge}_{Ge3d}) and Hf 4f core level (E^{Hf}_{Hf4f}) spectra of 1 nm thin HfO_2 film/(110)Ge interface, and (b) the CL spectrum of 5 nm HfO_2 film. The band gap of HfO_2 was determined to be 5.61 ± 0.1 eV.

B. HfO_2/(110)Ge heterointerface

As discussed earlier, the (110)Ge orientation has a significant effect on the hole mobility enhancement. The ΔE_V and ΔE_C discontinuities at the HfO_2/(110)Ge heterointerface were quantified using Eqs. (1) and (2). Figures 3(a) and 3(b) show the Ge 3d CL spectrum and VBM of (110)Ge film as well as Hf 4f CL spectrum and VBM of 5 nm HfO_2 film,

TABLE I. CL to VBM binding-energy difference for HfO_2 and epitaxial (100)Ge grown on (100)/6° GaAs substrate.

		Measured band offsets of HfO_2/(100)Ge/(100)GaAs	
Material and interface	Binding energy difference	ΔE_V (eV)	ΔE_C (eV)
Ge	$E^{Ge}_{Ge3d} - E^{Ge}_{VBM} = 29.45 \pm 0.05$ eV		
5 nm HfO_2	$E^{Hf}_{Hf4f} - E^{Hf}_{VBM} = 14.08 \pm 0.05$ eV		
1 nm HfO_2 on Ge	$E^{Hf}_{Hf4f} - E^{Ge}_{Ge3d} = 12.57 \pm 0.05$ eV		
E_g of HfO_2	5.52 ± 0.1 eV	2.8 ± 0.05	2.05 ± 0.1

TABLE II. CL to VBM binding-energy difference for HfO_2 and epitaxial (110)Ge grown on (110)GaAs.

		Measured band offsets of HfO_2/(110)Ge/(110)GaAs	
Material and interface	Binding energy difference	ΔE_V (eV)	ΔE_C (eV)
Ge	$E^{Ge}_{Ge3d} - E^{Ge}_{VBM} = 29.36 \pm 0.05$ eV		
5 nm HfO_2	$E^{Hf}_{Hf4f} - E^{Hf}_{VBM} = 14.50 \pm 0.05$ eV		
1 nm HfO_2 on Ge	$E^{Hf}_{Hf4f} - E^{Ge}_{Ge3d} = 12.58 \pm 0.05$ eV		
E_g of HfO_2	5.61 ± 0.1 eV	2.28 ± 0.05	2.66 ± 0.1

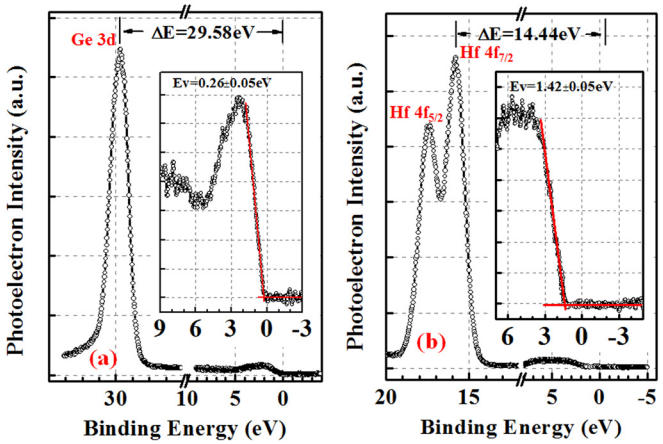

FIG. 5. XPS spectra of (a) Ge 3d core level (E^{Ge}_{Ge3d}) and valence band maximum, VBM (E^{Ge}_{VBM}) of (111)Ge film; (b) Hf 4f core level (E^{Hf}_{Hf4f}) spectrum and VBM (E^{Hf}_{VBM}) of 5 nm HfO_2 film.

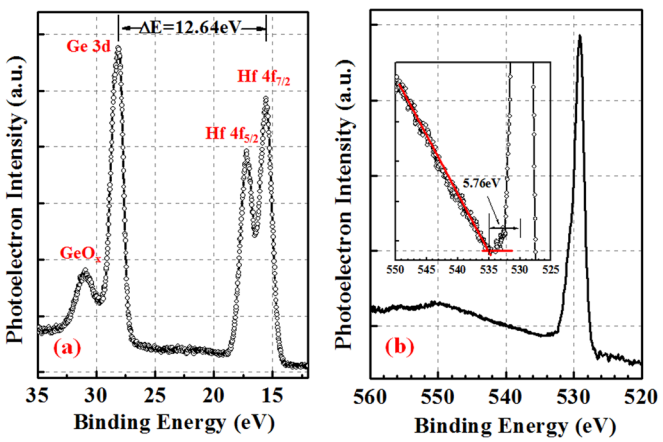

FIG. 6. XPS spectra of (a) Ge 3d (E^{Ge}_{Ge3d}) and Hf 4f core level (E^{Hf}_{Hf4f}) spectra of 1 nm thin HfO_2 film/(111)Ge interface, and (b) the CL spectrum of 5 nm HfO_2 film. The band gap of HfO_2 was determined to be 5.76 ± 0.1 eV.

respectively. Figure 4(a) shows the Ge 3d CL and Hf 4f CL spectrum of 1 nm HfO_2 on (110)Ge heterointerface. Figure 4(b) shows the CL spectrum of 5 nm HfO_2 film and the band gap was determined to be 5.61 ± 0.1 eV. The measured values of ΔE_v and ΔE_c at the HfO_2 on (110)Ge heterointerface were 2.28 ± 0.05 eV and 2.66 ± 0.1 eV, respectively, thus have a potential advantage for hole confinement. These band offset parameters were presented in Table II.

TABLE III. CL to VBM binding-energy difference for HfO_2 and epitaxial (111)Ge grown on (111)A GaAs.

Material and interface	Binding energy difference	Measured band offsets of HfO_2/(111)Ge/(111)A GaAs ΔE_V (eV)	ΔE_C (eV)
Ge	$E^{Ge}_{Ge3d} - E^{Ge}_{VBM} = 29.58 \pm 0.05$ eV		
5 nm HfO_2	$E^{Hf}_{Hf4f} - E^{Hf}_{VBM} = 14.44 \pm 0.05$ eV		
1 nm HfO_2 on Ge	$E^{Hf}_{Hf4f} - E^{Ge}_{Ge3d} = 12.64 \pm 0.05$ eV		
E_g of HfO_2	5.76 ± 0.1 eV	2.50 ± 0.05	2.59 ± 0.1

TABLE IV. Band offset values of HfO_2 on crystallographically oriented epitaxial Ge layers.

	(100)Ge	(110)Ge	(111)Ge
ΔE_v (eV)	2.8 ± 0.05	2.28 ± 0.05	2.50 ± 0.05
ΔE_c (eV)	2.05 ± 0.1	2.66 ± 0.1	2.59 ± 0.1
E_g of HfO_2 (eV)	5.52 ± 0.1	5.61 ± 0.1	5.76 ± 0.1

C. HfO_2/(111)Ge heterointerface

Figures 5 and 6 show the CL XPS spectra for the (111)Ge epitaxial layer, 5 nm HfO_2, 1 nm HfO_2 on (111) Ge interface, and HfO_2 bandgap, respectively. The measured

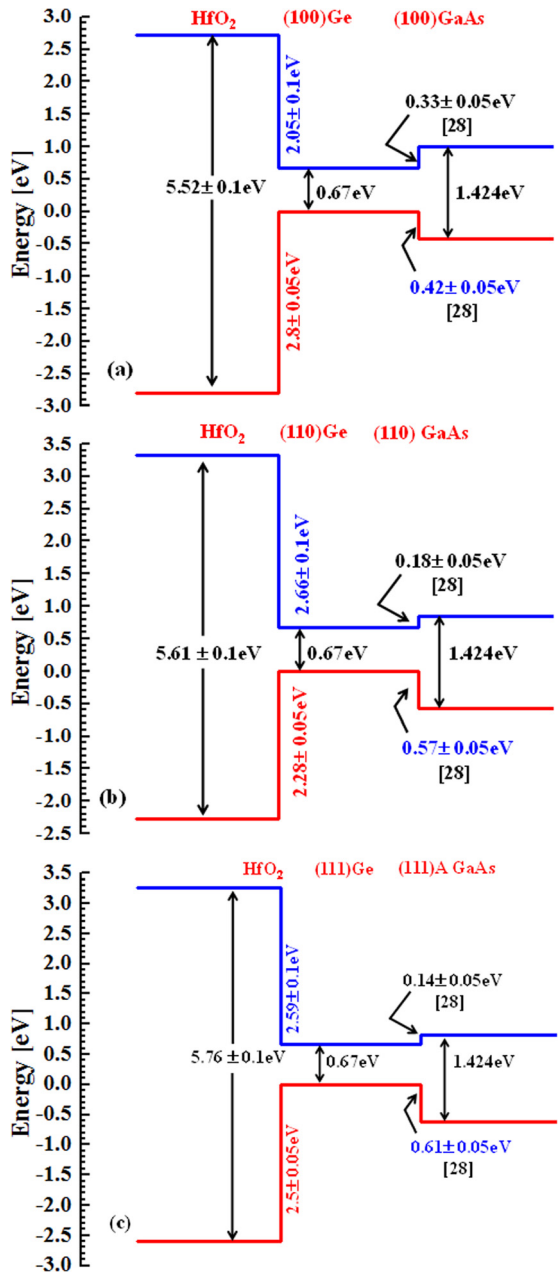

FIG. 7. Energy-band diagram of the HfO_2/Ge heterojunction obtained from XPS measurements on (a) (100)Ge, (b) (110)Ge, and (c) (111)Ge. The ΔE_c has been calculated based on the measured ΔE_v and the difference in bandgap of HfO_2 and Ge in each orientation, where $\Delta E_g = \Delta E_v + \Delta E_c$. The Ge/GaAs band offset in each orientation is included from Ref. 28.

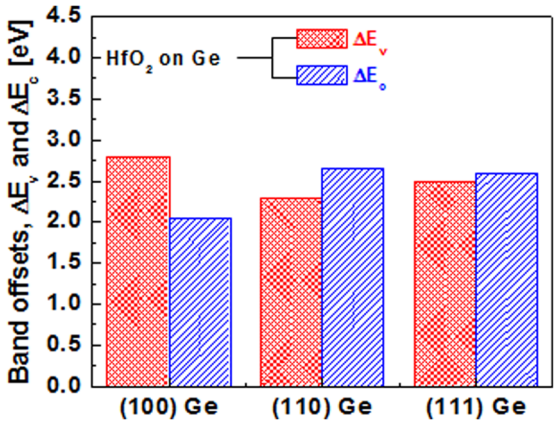

FIG. 8. Histogram of band offset distribution obtained from HfO_2/Ge heterointerface on crystallographically oriented epitaxial Ge layers.

values of ΔE_v and ΔE_c for the HfO_2 on (111)Ge were 2.50 ± 0.05 eV and 2.59 ± 0.1 eV, respectively. The result obtained from analysis of these data is presented in Table III. Although the magnitude of the variation of the ΔE_v and ΔE_c was consistent to the values on (100)Ge epilayer by other researchers, our results demonstrated a valence band offset relation of $\Delta E_V(100)Ge > \Delta E_V(111)Ge > \Delta E_V(110)Ge$ and the conduction band offset relation of $\Delta E_c(110)Ge > \Delta E_c(111)Ge > \Delta E_c(100)Ge$ after careful investigation of HfO_2 on crystallographically oriented epitaxial Ge layers by XPS measurements. The result obtained from this analysis is also presented in Table IV. One can find that the crystallographic orientation of Ge epilayer has a strong influence on the band offset properties, which is believed to be the quality of the Ge/GaAs heterojunction growth, the surface reconstruction of Ge layer, and the interface quality of the HfO_2/Ge heterointerface. Figure 7 shows the band alignment diagram of the measured HfO_2 on (a) (100)Ge, (b) (110)Ge, and (c) (111)Ge heterointerface. The band offset values of Ge on (100)GaAs, (110)GaAs, and (111)A GaAs substrates were included in this figure from Ref. 28. Although the transport properties strongly depend on the interface states between the high-κ and the Ge layer, there are no reliable bandgap data of GeO_x ($1 \leq x \leq 2$) which are available. Therefore, the only measured band alignment of HfO_2 on crystallographically oriented epitaxial Ge is included in Fig. 7. Figure 8 shows the histogram of ΔE_v and ΔE_c distribution obtained from atomic layer HfO_2 oxide film deposited on crystallographically oriented Ge layers. One can find from this figure that the measured valence and conduction band offsets were above 2 eV, required for confining carriers inside the Ge channel to reduce the leakage current. Thus, these measured band offset values on crystallographically oriented epitaxial Ge will provide a promising path for Ge based n-channel and p-channel transistor design.

IV. CONCLUSIONS

Epitaxial crystallographically oriented Ge layers were grown by *in situ* MBE growth process on (100), (110), and (111)A GaAs substrates. Atomic layer HfO_2 oxide films were deposited on each Ge film. The band alignment properties of HfO_2 on epitaxial crystallographically oriented Ge layers were investigated using x-ray photoelectron spectroscopy. Valence band offsets of 2.8 eV, 2.28 eV, and 2.5 eV were measured from HfO_2/(100)Ge, HfO_2/(110)Ge, and HfO_2/(111)Ge heterointerfaces, respectively, using XPS measurement. Using XPS data, variations in valence band offset $\Delta E_V(100)Ge > \Delta E_V(111)Ge > \Delta E_V(110)Ge$ related to crystallographic Ge were obtained. Moreover, the conduction band offset related to the crystallographic Ge was $\Delta E_c(110)Ge > \Delta E_c(111)Ge > \Delta E_c(100)Ge$ using the measured bandgap of HfO_2 on each orientation and with the Ge bandgap of 0.67 eV. These band offset parameters for carrier confinement would offer an important guidance for designing Ge-based p-and n-channel metal-oxide field-effect transistor for low-power application.

ACKNOWLEDGMENTS

This work is supported in part by Intel Corporation.

[1]International Technology Roadmap for Semiconductors (ITRS), *Process Integration, Devices and Structures (PIDS)*, 2011 ed. (ITRS, 2011).
[2]M. K. Hudait, ECS Trans. **45**, 581 (2012).
[3]M. K. Hudait, G. Dewey, S. Datta, J. M. Fastenau, J. Kavalieros, W. K. Liu, D. Lubyshev, R. Pillarisetty, W. Rachmady, M. Radosavljevic, T. Rakshit, and R. Chau, in *IEEE Conference Proceedings of International Electron Devices Meeting (IEDM)* (IEEE, New York, 2007), p. 625.
[4]M. Radosavljevic, T. Ashley, A. Andreev, S. D. Coomber, G. Dewey, M. T. Emeny, M. Fearn, D. G. Hayes, K. P. Hilton, M. K. Hudait, R. Jefferies, T. Martin, R. Pillarisetty, W. Rachmady, T. Rakshit, S. J. Smith, M. J. Uren, D. J. Wallis, P. J. Wilding, and R. Chau, in *IEEE Conference Proceedings of International Electron Devices Meeting (IEDM)* (IEEE, New York, 2008), p. 727.
[5]R. Pillarisetty, B. Chu-Kung, S. Corcoran, G. Dewey, J. Kavalieros, H. Kennel, R. Kotlyar, V. Le, D. Lionberger, M. Metz, N. Mukherjee, J. Nah, W. Rachmady, M. Radosavljevic, U. Shah, S. Taft, H. Then, N. Zelick, and R. Chau, in *IEEE Conference Proceedings of International Electron Devices Meeting (IEDM)* (IEEE, New York, 2010), p. 150.
[6]Y. Sun, S. E. Thompson, and T. Nishida, *Strain Effect in Semiconductors: Theory and Device Applications*, 1st ed. (Springer, 2009).
[7]M. V. Fischetti and S. E. Laux, J. Appl. Phys. **80**, 2234 (1996).
[8]J. Kim and M. V. Fischetti, J. Appl. Phys. **108**, 013710 (2010).
[9]Y. Sun, S. E. Thompson, and T. Nishida, J. Appl. Phys. **101**, 104503 (2007).
[10]S. Dissanayake, Y. Zhao, S. Sugahara, M. Takenaka, and S. Takaghi, J. Appl. Phys. **109**, 033709 (2011).
[11]T. Low, M. F. Li, G. Samudra, Y. Yeo, C. Zhu, A. Chin, and D. Kwong, IEEE Trans. Electron Devices **52**, 2430 (2005).
[12]T. Krishnamohan, D. Kim, T. V. Dinh, A. Pham, B. Meinerzhagen, C. Jungemann, and K. Saraswat, in *IEEE Conference Proceedings of International Electron Devices Meeting (IEDM)* (IEEE, New York, 2008), p. 899.
[13]S. Dissanayake, K. Tomiyama, S. Sugahara, M. Takenaka, and S. Takagi, Appl. Phys. Express **3**, 041302 (2010).
[14]S. Nakaharai, T. Tezuka, N. Sugiyama, Y. Moriyama, and S. Takagi, Appl. Phys. Lett. **83**, 3516 (2003).
[15]M. Bohr, in *IEEE Conference Proceedings of International Electron Devices Meeting (IEDM)* (IEEE, New York, 2011), p. 1.1.1.
[16]J. Robertson and B. Falabretti, J. Appl. Phys. **100**, 014111 (2006).
[17]J. H. Choi, Y. Mao, and J. P. Chang, Mater. Sci. Eng. R. **72**, 97 (2011).
[18]M. Perego, G. Seguini, and M. Fanciulli, J. Appl. Phys. **100**, 093718 (2006).
[19]S. J. Wang, A. C. H. Huan, Y. L. Foo, J. W. Chai, J. S. Pan, Q. Li, Y. F. Dong, Y. P. Feng, and C. K. Ong, Appl. Phys. Lett. **85**, 4418 (2004).
[20]H. Seo, F. Bellenger, K. B. Chung, M. Houssa, M. Meuris, M. Heyns, and G. Lucovsky, J. Appl. Phys. **106**, 044909 (2009).
[21]S. Swaminathan, Y. Sun, P. Pianetta, and P. C. McIntyre, J. Appl. Phys. **110**, 094105 (2011).
[22]M. K. Hudait, Y. Zhu, D. Maurya, S. Priya, P. K. Patra, A. W. K. Ma, A. Aphale, and I. Macwan, J. Appl. Phys. (submitted).

[23]S. Y. Chiam, W. K. Chim, C. Pi, A. C. H. Huan, S. J. Wang, J. S. Pan, S. Turner, and J. Zhang, J. Appl. Phys. **103**, 083702 (2008).
[24]H. Shang, H. Okorn-Schimdt, J. Ott, P. Kozlowski, E. C. Jones, H.-S. P. Wong, and W. Hanesch, IEEE Electron Device Lett. **24**, 242 (2003).
[25]W. E. Spicer, I. Lindau, P. Skeath, C. Y. Su, and P. Chye, Phys. Rev. Lett. **44**, 420 (1980).
[26]P. Chiaradia, M. Fanfoni, P. Nataletti, P. De Padova, L. J. Brillson, M. L. Slade, R. E. Viturro, D. Kilday, and G. Margaritondo, Phys. Rev. B **39**, 5128 (1989).
[27]M. K. Hudait, Y. Zhu, N. Jain, S. Vijayaraghavan, A. Saha, T. Merritt, and G. A. Khodaparast, J. Vac. Sci. Technol. B **30**, 051205 (2012).
[28]M. K. Hudait, Y. Zhu, N. Jain, and J. L. Hunter, Jr., J. Vac. Sci. Technol. B **31**, 011206 (2013).
[29]E. A. Kraut, R. W. Grant, J. R. Waldrop, and S. P. Kowalczyk, Phys. Rev. Lett. **44**, 1620 (1980).
[30]C. Jia, Y. Chen, Y. Guo, X. Liu, S. Yang, W. Zhang, and Z. Wang, Nanoscale Res. Lett. **6**, 316 (2011).
[31]S. A. Chambers, T. Droubay, T. C. Kaspar, and M. Gutowski, J. Vac. Sci. Technol. B **22**, 2205 (2004).
[32]S. Spiga, C. Wiemer, G. Scarel, G. Seguini, M. Fanciulli, A. Zenkevich, and Y. Lebedinskii, in *Advanced Gate Stacks for High-Mobility Semiconductors*, edited by A. Dimoulas, E. Gusev, P. C. McIntyre, and M. Heyns (Springer, Berlin, 2007).